Thermal quench effects on ferroelectric domain walls

P. Paruch,[1,*] A. B. Kolton,[2] X. Hong,[3,†] C. H. Ahn,[3] and T. Giamarchi[1]

[1]*DPMC-MaNEP, Université de Genève, 24 Quai Ernest Ansermet, 1211 Geneva, Switzerland*
[2]*CONICET, Centro Atómico Bariloche, 8400 San Carlos de Bariloche, Río Negro, Argentina*
[3]*DAP, Yale University, P. O. Box 208284, New Haven, Connecticut 06520-0284, USA*

Using piezoresponse force microscopy on epitaxial ferroelectric thin films, we have measured the evolution of domain wall roughening as a result of heat-quench cycles up to $735\,^{\circ}$C, with the effective roughness exponent ζ changing from 0.25 to 0.5. We discuss two possible mechanisms for the observed ζ increase: a quench from a thermal one-dimensional configuration and from a locally equilibrated pinned configuration with a crossover from a two- to one-dimensional regime. We find that the postquench spatial structure of the metastable states, qualitatively consistent with the existence of a growing dynamical length scale whose ultraslow evolution is primarily controlled by the defect configuration and heating process parameters, makes the second scenario more plausible. This interpretation suggests that pinning is relevant in a wide range of temperatures and, in particular, that purely thermal domain wall configurations might not be observable in this glassy system. We also demonstrate the crucial effects of oxygen vacancies in stabilizing domain structures.

I. INTRODUCTION

Domain walls separating differently polarized regions in ferroelectric thin films present a powerful model system in which the characteristic roughening and complex dynamics resulting from competing elastic and pinning forces can be readily accessed.[1] Understanding this behavior is key to the physics of many diverse disordered elastic systems (DES)[2–9] and of significant technological interest for memory and electromechanical ferroelectric applications[10–12] and devices using the domain walls as nanoscale functional components,[13,14] in which control over the stability and growth of domain structures is of paramount importance.

Theoretically, although equilibrium DES properties are relatively well understood, much less is know about the out-of-equilibrium behavior of these systems. A major challenge is understanding the nonsteady slow dynamics associated with aging.[15–17] An especially interesting realization of such out-of-equilibrium phenomena is provided by quenches, in which a parameter is abruptly varied. The study of such quenches is a challenge not only for classical systems but also for quantum systems.[18,19] For classical systems, studies of interfaces subjected to quenches[20–24] have shown aging of the interface and a long-term memory of the initial configuration.

On the experimental side, studies of ferroelectric domain walls in the DES framework have so far focused mostly on equilibrium properties, with switching current and dielectric measurements showing domain wall pinning in bulk ferroelectrics[25] and random-field disorder inferred for relaxors,[26] while piezoforce microscopy (PFM) studies of domain wall roughening and creep reported strong dipolar interactions and random bond disorder in epitaxial ferroelectric thin films.[27–29] Unlike their theoretical counterparts, these systems also show pinning by individual strong defects[30] and local variations of both disorder strength and universality class,[31] further complicating the approach to nonequilibrium behavior. Thermal effects in bulk[32] and thin film materials[33] include increased roughness and higher domain wall mobility on heating and transition to domain wall depinning at lower

temperatures.[34] However, a detailed nanoscale analysis of the complex behavior associated with a thermal quench of these systems remains an open question.

In this paper we report on PFM measurements of domain walls in ferroelectric $Pb(Zr_{0.2}Ti_{0.8})O_3$ (PZT) thin films, heat-quench cycled up to $735\,^{\circ}$C, in which the value of the roughness exponent ζ, reflecting the system dimensionality and the nature of the disorder, is extracted from an analysis of the domain wall position and evolves from $\sim$0.25 to $\sim$0.5. Despite the similarity of the measured exponent with the thermal $\zeta_{\mathrm{th}} = 1/2$ in one dimension, we show that the observed behavior cannot result from the quench of an initial high-temperature thermal configuration, as the observed roughness values are much higher than would be expected in this scenario. Rather, it is clear that disorder pinning continues to dominate the behavior during the quench, with one possibility being that the domain walls cross from a two- to one-dimensional regime. We also follow the complex thermal evolution of circular nanoscale ferroelectric domains, in which the combined effects of disorder pinning, line tension, and a preferential polarization orientation can be observed and the crucial effects of oxygen vacancies in stabilizing domain structures are highlighted.

II. MATERIALS AND METHODS

Thermal quench studies were carried out on c-axis-oriented PZT films, epitaxially grown on single crystal (001) $Nb:SrTiO_3$ substrates at $\sim$500 $^{\circ}$C by off-axis radiofrequency magnetron sputtering, in an Ar-O_2 process gas mixture,[35] with high crystal and surface quality confirmed by x-ray diffraction and atomic force microscopy (AFM). In these films, the polarization vector along the c axis can be locally switched by a biased AFM tip, using the substrate as a ground electrode, and the resulting ferroelectric domains imaged by PFM.[36] To study the effects of heat-quench cycling on domain wall roughness we wrote $10 \times 10\ \mu m^2$ arrays of linear 1-μm-wide domains with ± 12 V alternately applied to a scanning AFM tip. To explore the interaction among heating, line tension,

and disorder pinning, we wrote arrays of nanoscale circular domains with ± 12 V pulses of different duration in a uniform, oppositely polarized region. The films were heated in air to progressively higher temperatures for fixed time intervals and then quenched to room temperature on a large copper block. Ambient temperature PFM images of the evolving domain structures were acquired after each heating-quench cycle. In addition, to investigate the role of oxygen vacancies on domain stability, films grown under the same conditions but cooled in process gas, Ar, or O_2 were compared.

As in our previous work,[28] to extract the correlation function of relative displacements $B(L)$ for a given PFM phase image of linear domains, we first isolated a single domain wall and then binarized the image using a cutoff extracted from the midway point between the phase contrast values for the two polarization orientations. The elastically optimal flat domain wall position was determined from a least-squares linear fit to the binarized image, which finally allowed the extraction of the relative displacements and their correlation at different length scales. To compensate for possible effects of scanner drift, for each set of walls, PFM measurements taken in an "up" versus "down" scan direction were averaged. Although ambient-condition walls after writing were generally well defined, repeated heat-quench cycles, especially close to T_C, led to the appearance of multivalued features such as bubbles or overhangs. In some cases, such features could also be present even immediately after writing at room temperature. Bubbles, being very small, well-defined domains of opposite contrast near but not coincident with the position of the primary domain wall, could be removed from the binarized image by hand. For overhangs, the algorithm used to calculate relative displacements would simply result in a renormalized single value "effective position" of the domain wall. Therefore, when such features became prevalent, or when the films switched to the preferred polarization direction on heating near T_C, quantitative analysis could no longer be carried out, as indicated by the symbol x in Table I.

III. DOMAIN WALL ROUGHNESS

Generally, an elastic manifold in the absence of disorder and thermal fluctuations (0 K temperature) would take an ideally flat configuration in order to optimize its energy. Random variations in the potential landscape, whether due to disorder or thermal fluctuations, allow further optimization as the manifold wanders between particularly favorable regions in the potential, giving rise to a characteristic roughening. In the case of single manifold, an interface such as a domain wall, contact line, or fracture, fully in equilibrium with its random potential landscape, the resulting geometrical fluctuations from an elastically optimal flat configuration are present at all length scales, with the system showing monoaffine scaling properties (for a more detailed presentation, see Ref. 2 and references therein). The key quantity describing this roughening is the correlation function,

$$B(L) = \overline{\langle [u(z+L) - u(z)]^2 \rangle} \propto L^{2\zeta}, \tag{1}$$

known as the roughness function. Here $u(z)$ are the transverse displacements along the longitudinal coordinate z with respect to a flat configuration, measured a distance L apart on the interface, and $\langle \ldots \rangle$ and $\overline{\cdots}$ the thermal and disorder averages, respectively. The value of the roughness exponent ζ depends on the dimensionality of the system, the nature of the disorder potential, and the range of the elastic interactions. Extracting ζ not only yields this important information, which may be used to determine the universality class of the disorder and the dominant pinning defects present in the system, but also allows a full scaling prediction of the complex nonlinear creep response of such systems to small driving forces.[27] We have previously shown for linear domains created artificially by straight-line scanning with a biased AFM tip that, as a result of this writing process, the domain walls are essentially flat at large length scales, with roughening observed only at short length scales, probably where the stray fields during the writing process allow some small accommodation to the potential landscape.[28] The experimentally obtained $B(L)$ thus shows a power-law growth at short length scales, from which the roughness exponent ζ can be extracted, followed by a saturation at large length length scales.

As previously reported in Ref. 33, linear domains in process-gas-cooled films show very high stability on heating, with increased roughness only at small length scales [Figs. 1(a)–1(f)]. At 625°–785 °C (depending on the sample), close to the Curie temperature T_C of the films determined by x-ray diffraction,[37] extensive polarization switching occurs and the written domains eventually disappear as the region reverts to its as-grown monodomain state. Quasi-identical behavior was observed in the Ar-cooled samples [Figs. 1(m)–1(o)]. In the O_2-cooled films, however, the domain structures showed much lower thermal stability. In these films, expected to show decreased oxygen vacancy densities compared to process-gas or Ar-cooled samples, increased roughening was found even for short (20-min) heating intervals, with domain disappearance observed already at 250°–350 °C [Figs. 1(j)–1(l)]. Nonetheless, x-ray measurements confirmed sample T_C in the 600°–700 °C range, similarly to those of the process-gas-cooled samples.[37]

TABLE I. Thermal evolution of the roughness exponent ζ for PZT films cooled in process gas (PG), argon (Ar), and oxygen (O_2) after long (A: 1–3 h, P.P.) and short (B: 20–30 min, X.H.) heat-quench cycles. —, data set missing or noisy. x, temperatures beyond domain disappearance, multivalued wall roughness configuration. *225 °C measurement.

(A) Film	T(°C)							
	25	110	200	285	385	485	585	685
50-nm PG	0.33	0.43	0.42	0.48	0.54	0.50	0.51	0.45
91-nm PG	0.23	0.22	0.35	–	0.37	0.39	x	x
52-nm PG	0.26	0.26	0.18	0.23	0.26	0.31	0.45	x

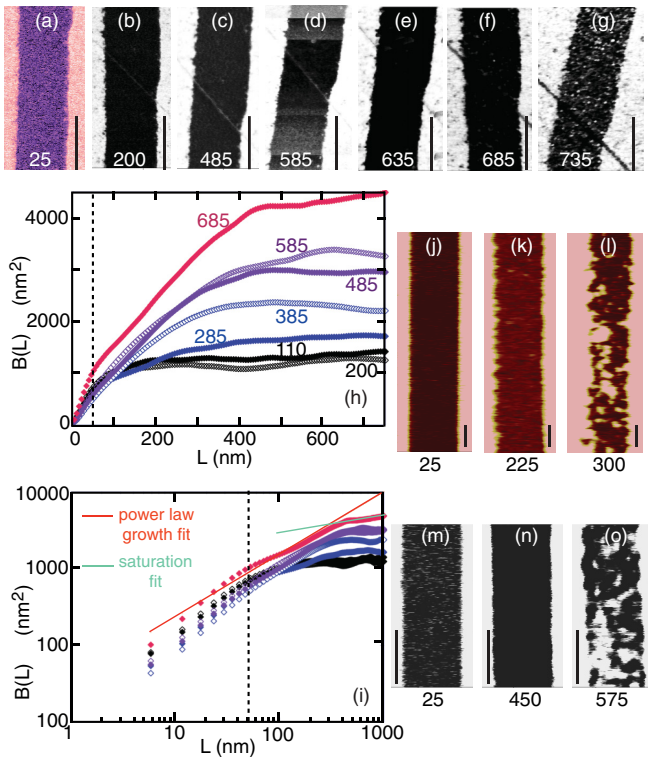| (B) Film	T(°C)							
	25	200	300	400	475	500	575	600
50-nm PG	0.10	0.15	0.31	0.30	0.27	0.42	x	x
40-nm PG	0.24	–	0.29	0.29	–	0.24	0.42	0.50
40-nm Ar	0.27	0.18	0.17	0.27	–	0.22	0.38	0.41
100-nm O_2	0.15	0.45*	0.47	x	x	x	x	x

FIG. 1. (Color online) PFM images of linear ferroelectric domains in a process-gas-cooled 50-nm PZT film (a) immediately after writing and [(b)–(g)] after thermal cycling to the indicated temperatures (°C). Similar measurements [(j)–(l)] in an O_2-cooled 100-nm film and [(m)–(o)] an Ar-cooled 40-nm film, where higher oxygen vacancy densities appear to stabilize the domain walls. Vertical 1-μm scale bars are shown in all images. (h) Average $B(L) = \langle [u(z + L) - u(z)]^2 \rangle$ extracted after thermal cycling to the indicated temperatures (°C) for all the domain walls in the 50-nm film. (i) The power-law growth region of $B(L)$ for same measurement (identical color code for the temperatures). The extrapolated fit to the power-law growth region of $B(L)$ (first 20 points) with $\ln[B(L)] \propto 0.890 \ln[L]$ is shown in dark gray (red), and the fit to the saturation region of $B(L)$ in light gray (aquamarine) for the 685° data set. The intersection of these fits allows the saturation length scale $L^\star$ to be extracted. The dashed vertical line in (h) and (i) indicates the length scale L equal to the film thickness.

To quantitatively examine the roughness evolution, for each sample we extracted the average roughness function $B(L)$. For the relatively flat, as-written domain walls before thermal cycling, as in our previous studies,[28] we find a power-law growth of $B(L)$ at short length scales followed by saturation at $L^\star \sim 25$–100 nm (comparable to the ~ 40- to 100-nm film thickness), with $B(L^\star) \sim 100$–1000 nm^2 in the different films. After heating, the power-law-growth region of $B(L)$ extends to $L^\star \sim 300$–700 nm and the saturation value increases $[B(L^\star) \sim 1000$–$10\,000$ nm$^2]$, consistent with the observed increase in domain wall roughness [Figs. 1(h) and 1(i)]. From the power-law growth region of $B(L)$ [Fig. 1(l)], we extract a value for the roughness exponent ζ, characterizing the static equilibrium configuration of the domain wall in the random manifold regime, where $B(L) \propto L^{2\zeta}$. As shown in Table I for domain walls in different films, heating increases the

value of ζ from ~ 0.25 at ambient conditions and lower temperature thermal cycling to ~ 0.5 at higher temperatures and near domain disappearance.[38] In O_2-cooled films, higher roughness and increased ζ values are seen already at relatively low temperatures.

IV. DISCUSSION

To understand these data, we first consider the thermal roughening of the linear domain walls within the theoretical framework of DES. Our previous studies have shown that at ambient conditions with no applied electric field, thermal excitations alone are not enough to overcome the energy barriers between different metastable states in the duration of the experiment, although the electric field applied during writing allows domain walls to accommodate at short length scales to the surrounding random potential landscape. A power-law growth of $B(L)$ is, thus, observed only at length scales smaller than the film thickness, where the domain wall behavior agrees well with theoretical predictions for two-dimensional interfaces pinned by weak, collective random bond disorder and in the presence of long-range dipolar forces.[28,39] Given the finite thickness of the sample, much smaller than its lateral dimensions, it is reasonable to expect that in a weak collective pinning scenario, were the walls to fully equilibrate, one-dimensional behavior would be evident at large length scales. Although it is difficult to estimate the exact length scale $L_\times$ for such a two-dimensional-to-one-dimensional crossover in a disordered system, we can expect it to be of the order of the sample thickness. This would be exactly the case for purely thermal roughening. The increased energy provided to the samples on thermal cycling to progressively higher temperatures is one way to promote further equilibration of the domain walls, allowing them to accommodate to the surrounding potential landscape at length scales greater than the film thickness, where the one-dimensional nature of the domain walls should become evident.

If thermal roughening dominates in the high-temperature one-dimensional regime, the walls should be characterized by a roughness exponent $\zeta_{th} = 1/2$ and slowly age to the equilibrium ζ_{eq} configuration when quenched. For an increasing time t after the quench, a growing length $L_{dyn}(t)$ should, thus, separate the equilibrated short length scales (with exponent ζ_{eq}) from the large scales conserving a memory of the roughness at the quench (with exponent ζ_{th}), analogously to a quench from an initially flat configuration.[20] We confirmed such a scenario in Langevin dynamics simulations of a one-dimensional interface in a random medium as detailed in Ref. 20, but this time quenching an initially equilibrated high-temperature configuration. The results indeed show the quasifreezing of this initial configuration at the largest length scales, with thermally activated dynamic evolution distinguishable only at very small length scales [Fig. 2(a)]. This behavior is also reflected in the evolution of $B(L,t)$ after the quench [Fig. 2(b)]: At large lengths $L > L_{dyn}(t)$ we observe $B(L,t) \sim L^{2\zeta_{th}}$, while at small lengths the line tends to approach the equilibrium roughness exponent ζ_{eq} [with $\zeta_{eq} = 2/3$ for an elastic line with short range elasticity (random bond disorder)].

If the barriers are large, as the high stability of ferroelectric domain walls indicates, the length $L_{dyn}(t)$ can grow extremely
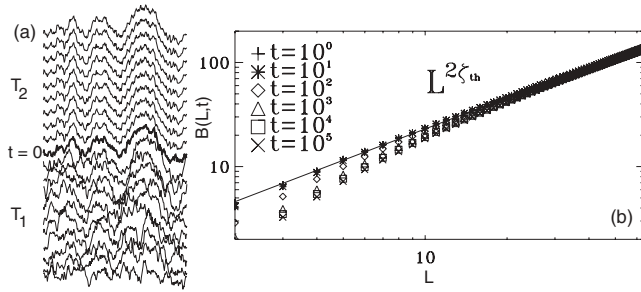
FIG. 2. Numerical simulation of an overdamped elastic string in a random medium undergoing a temperature quench $T_1 \rightarrow T_2 < T_1$ at $t = 0$. (a) From bottom to top: Typical evolution of the elastic string each 10 000 steps. The bold line is the configuration at the quench. (b) Curves from top to bottom: Evolution of the disorder-averaged correlation function of relative displacements $B(L,t)$ after the quench (symbols). The roughness exponent $\zeta_{th} = 0.5$ describes the geometry of the string at large length scales (solid line).

slowly, and most of the observable interface could well be characterized by the exponent $\zeta_{th} = 0.5$. This scenario seems consistent with the exponent $\zeta \sim 0.5$ observed at length scales up to 10 times greater than the thickness of the film. However, if we consider an elastic one-dimensional interface with energy $H = \frac{c}{2} \int dz (\nabla u)^2$, we obtain its thermal roughening at temperature T as

$$B(L) = \frac{k_B T}{c} \int_{-\infty}^{+\infty} dk \frac{1 - \cos(kL)}{2\pi k^2} = \frac{k_B T}{2c} |L|, \quad (2)$$

where the elastic constant c in the case of the domain wall is the product of its energy per unit area σ_{DW} and the film thickness d_f and k_B is the Boltzmann constant. Taking $\sigma_{DW} = 132$ mJm^{-2} from *ab initio* calculations for PbTiO$_3$,[40] we can, therefore, calculate the gradient $S = \frac{k_B T}{2c} = \frac{k_B T}{2\sigma_{DW} d_f}$ and the roughness $B(L^\star)_{th}$ expected for the thermal roughening scenario at the length scale corresponding to the experimentally observed saturation length $L^\star$. These values can be directly compared to the experimentally obtained values for the roughness $B(L^\star)_{exp}$ and the gradient $S_{exp} = B(L^\star)_{exp}/L^\star$ in the power-law-growth region where $B(L) \propto L^{2\zeta}$. As shown in Table II for the 50-nm PZT film of Fig. 1, the experimental $B(L)$ values are many orders of magnitude higher than those expected for a purely thermal roughening of a one-dimensional interface. The observed behavior at large length scales therefore cannot be simply a quench of the high-temperature

TABLE II. Comparison of the roughness function $B(L)$ and its gradient $S = \frac{k_B T}{2c}$ for a thermally roughened one-dimensional interface with the experimentally obtained gradient of $B(L) \propto L^{2\zeta}$ in a 50-nm PZT film.

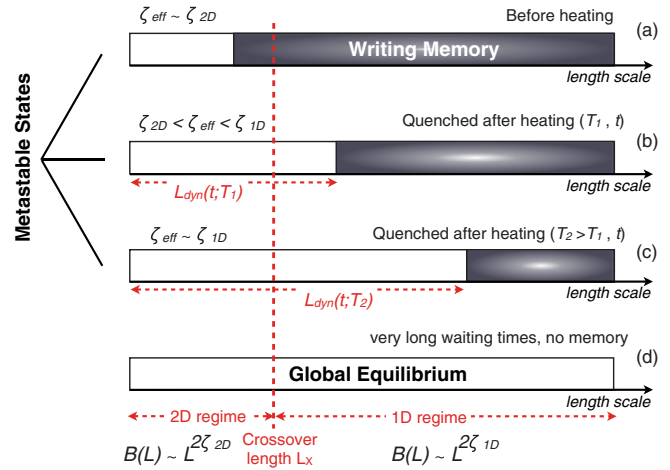| T (K)	383	473	558	658	758	858	958
$S \times 10^{-4}$ (nm)	4.0	4.9	5.8	6.9	7.9	9	10
$L^\star$ (nm)	58	121	72	180	199	200	232
$B(L^\star)_{th}$ (nm^2)	0.023	0.060	0.042	0.124	0.158	0.179	0.232
$B(L^\star)_{exp}$ (nm^2)	275	1593	1143	2805	3065	4089	4343
S_{exp} (nm)	4.8	13.1	15.8	15.5	15.4	20.5	188

FIG. 3. (Color online) Disorder dominated scenario as a function of length scale. (a) At ambient temperature before heating, the as-written, initially flat domain walls are only able to locally equilibrate at short length scales. [(b) and (c)] Heating facilitates thermally activated glassy relaxation and longer length scales become locally equilibrated as the heating temperature (or heating time) increases. (d) If fully in equilibrium (reference state), the system displays a two-dimensional to one-dimensional crossover at length scale $L_\times$, with no memory of the written state. This may be reflected by the effective roughness exponent ζ_{eff} in the correlation function $B(L) \sim L^{2\zeta_{eff}}$ of the quenched metastable states, as in (b) and (c), evolving from the two-dimensional value ζ_{1D}, when $L_{dyn} \leqslant L_\times$, toward the one-dimensional value ζ_{1D} when $L_{dyn} \gg L_\times$, especially if the crossover length scale is smeared out. In the 1D regime the "dynamical length" $L_{dyn}(t; T)$ is expected[20] to grow as $L_{dyn}(t; T) \sim [(T/U_0) \log(t/t_0)]^{1/\theta}$, with θ a positive exponent, U_0 a characteristic temperature, and t_0 a characteristic microscopic time. This prediction agrees qualitatively with the experimentally observed increase in ζ and $L^\star$ values with heating time and temperature.

configuration. Rather, pinning by disorder in the film continues to be the dominant effect, even during the quench.

One possible scenario is that of a dimensional crossover dominated by disorder: In equilibrium with a random bond disorder potential, below a typical length scale $L_\times$, comparable to the film thickness, the domain walls should act as two-dimensional elastic sheets with $\zeta_{2D} \simeq 0.2$–0.3 and as one-dimensional elastic strings with $\zeta_{1D} = 2/3$ for higher length scales [see Fig. 3(d)]. If this crossover is smeared out, it is not improbable that an effective $\zeta_\times : \zeta_{2D} < \zeta_\times < \zeta_{1D}$ is observed experimentally. According to the theory of DES,[20] the locally equilibrated regime just after the quench should extend up to a length scale that grows with the heating-time t and the heating temperature T, as the dynamical length $L_{dyn}(t) \sim [(T/U_0) \log(t/t_0)]^{1/\theta}$, with θ a positive exponent, U_0 a characteristic temperature, and t_0 a characteristic microscopic time. We then expect to observe equilibrium power-law behavior (possibly including the equilibrium dimensional crossover) below $L_{dyn}(t)$ and a memory of the flat initial condition, imposed by the linearly scanning AFM tip during writing, above it. The theory thus predicts a temperature dependence of the effective roughness exponent, from $\zeta_\times \sim \zeta_{2D}$ at low temperatures, $T : L_{dyn}(t; T) \sim L_\times$ [see Fig. 3(b)], to $\zeta_\times \sim \zeta_{1D}$ at higher temperatures $T : L_{dyn}(t; T) \gg L_\times$ [see Fig. 3(c)]

where the power-law behavior is effectively dominated by the equilibrium one-dimensional regime. The results displayed in Figs. 1(e) and 1(l) qualitatively agree with this theoretically expected scenario, and, in particular, the results in Table I are consistent with the expected heating-temperature dependence of the effective roughness exponent. The theory also predicts, at a fixed temperature, a slow (logarithmic) time dependence of $L_{\rm dyn}(t)$ that should translate into a heating-time dependence of $\zeta_\times$, from $\zeta_{\rm 2D}$ at short heating times $t : L_{\rm dyn}(t; T) \sim L_\times$, to $\zeta_{\rm 1D}$ at large times, $t : L_{\rm dyn}(t) \gg L_\times$, as summarized in Fig. 3. In this respect, the results shown in Table I for the 50-nm PG-cooled samples in (A) and (B) seem to be also qualitatively consistent with the theory.

Moreover, the $S_{\rm exp}$ values in Table II show no clear linear temperature dependence, a fact that is also qualitatively consistent with large length scales dominated by disorder and which we can further analyze through the following estimates. Phenomenologically, in the case of disorder-dominated roughening of an elastic interface,[2,41] we can consider in the two-dimensional regime at short length scales that $B(L) = r_f^2 (L/L_C)^{2\zeta(\rm 2D)}$, where r_f is the correlation length of the disorder potential and L_C is the Larkin length (minimum pinning length, below which the interface would behave purely elastically). In the one-dimensional regime at large length scales, this relation would become $B(L) = r_{\rm char}^2 (L/L_\times)^{2\zeta(\rm 1D)}$, where the characteristic length in this case would be the crossover length scale $L_\times$ and $r_{\rm char} = r_f (L_\times/L_C)^{\zeta(\rm 2D)}$. Taking $L_C \sim 0.2$ nm from 29, $\zeta(\rm 2D) = 0.25$, $\zeta(\rm 1D) = 0.5$, and $L_\times \sim d_f$ for the 50- and 91-nm samples, we find that the experimentally obtained $B(L)$ values would correspond to $r_f \sim 4$ nm in the two-dimensional regime (ambient conditions) and $r_f \sim 4$–8 nm in the one-dimensional regime (thermally cycled). For reference, the 10^{18}- to 10^{19}-cm^{-3} impurity densities extracted from current-voltage measurements in PZT films[42] correspond to an interdefect spacing of $\sim$4.5–10 nm and would, thus, qualitatively agree with the extracted disorder correlation lengths.

An additional important consideration, especially at increasing temperatures, is the exact nature of the disorder. Although surface deterioration is seen on heating, especially at the highest temperatures, x-ray characterization of the samples demonstrates continued high crystalline quality.[33] However, the mobility of point defects, such as oxygen vacancies, increases strongly with temperature. From the comparison of PG-, Ar-, and O$_2$-cooled films, it appears that the primary defects responsible for the domain wall pinning are indeed oxygen vacancies. These defects can appreciably lower their energy by associating with a domain wall,[43] so the probability of a migration and segregation of defects at the domain walls on thermal cycling, effectively increasing the strength of the pinning potential and stabilizing the domain structures against large-scale thermal roughening, is very high. In this respect, it is worth noting that in the theory of DES an analogous "slow structural relaxation" mechanism was very recently shown[44] to provide a minimal model for predicting pinning enhancement or aging of the static friction force and the phenomenon of "aftershocks" or static-relaxation-induced instabilities in the interface. This is interesting, as these phenomena are both absent in the standard DES models with truly quenched disorder, but they are, for instance, observed in solid friction experiments.

Another possibility is that the thermal cycling steps, by removing the water layer normally present on the film surface in air at ambient temperature, significantly affect the electrostatic boundary conditions and, thus, the effective potential landscape experienced by the domain walls. In this case, the higher roughness and increased ζ values could reflect the configuration adapted by the walls under these new conditions, and frozen-in after a quench from high temperature, possibly in parallel to a dimensional crossover. Further investigation would be needed to assess the potential importance of this effect and also to quantitatively test the scenario described above, summarized in Fig. 3.

V. DOMAIN SWITCHING AND GROWTH

The crucial role of disorder in stabilizing the domain walls in a given configuration is further highlighted by the behavior of nanoscale circular domains followed in parallel measurements during the same heat-quench cycles. In these measurements, we note the strong polarization switching asymmetry: P$_{\rm DOWN}$ domains written with positive tip voltage in a negatively prepolarized area grow significantly larger for a given pulse duration [Figs. 4(a)–4(f)], even in films P$_{\rm UP}$ polarized as grown. We relate this feature to the highly asymmetric device configuration.[45,46] In PG- and Ar-cooled films at ambient temperature, both tip voltage polarities give uniform, circular domains, which become irregular on heating, with apparent bowing of the domain walls. In P$_{\rm UP}$ as-grown films, P$_{\rm DOWN}$ domains decrease in size after thermal cycling, while in P$_{\rm DOWN}$ as-grown films a slight increase in domain size was observed. Some of the smaller domains (20- to
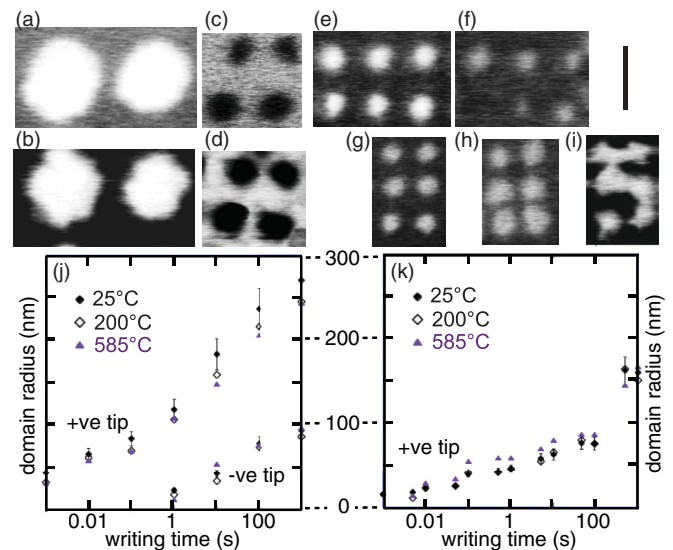

FIG. 4. PFM images of nanoscale ferroelectric domains written at ambient conditions in the 91-nm PZT film (P$_{\rm UP}$ as grown) with (a) 1-s, +12-V, (c) 10-s, −10-V, (e) 1-ms, +12-V pulses, and in a 52-nm PZT film (P$_{\rm DOWN}$ as grown) with (g) 100-ms, +12-V pulses. Domain evolution after thermal cycling [(f) and (h)] to 200 °C and [(b), (d), and (i)] 585 °C. Vertical bar = 250 nm. All images are shown to the same scale. The average domain size as a function of the writing time at ambient conditions, and after thermal cycling up to the indicated temperatures (j) for the 91-nm film and (k) for the 52-nm film.

50-nm radius) of both polarities collapse even after low-temperature heating intervals [Figs. 4(e) and 4(f)]. In P_{DOWN} as-grown films, significant displacements and an "amoeboid-like" growth are observed for P_{DOWN} domains near T_C, with the structures eventually coalescing [Figs. 4(g)–4(i)]. In the O_2-cooled films, even at ambient conditions P_{UP} domains were unstable and P_{DOWN} domains were stable only for domain radii greater than $\sim$100 nm.

This complex thermal evolution can be understood by considering the forces on the domain wall due to its curvature and the polarization orientation as well as disorder and thermal effects. A preferred monodomain state indicates an asymmetry of the ferroelectric double well potential, which promotes growth or collapse of domains depending on their polarization orientation. In addition, the "line tension" or elastic energy cost of circular domain walls promotes domain collapse, its effects diminishing with increasing domain size. Finally, disorder allows domain wall pinning and, therefore, deformations from the elastically optimal circular geometry. The relative strength of these contributions during thermal cycling can be gauged from the degree of domain stability. Although polarization orientation and device asymmetry[47] determine the domain size for a given writing time, for domains of comparable size, line tension determines stability. Larger P_{UP} and P_{DOWN} domains remain, while 20- to 50-nm radius domains readily collapse on heating. Domain wall roughening is observed for all domain sizes, although the extent of the deformations increases with domain size. Disorder appears to be crucial in stabilizing the domain structures, in particular the smallest domains, and protects them against thermal effects.

VI. CONCLUSION

In conclusion, our studies show that in epitaxial ferroelectric thin films, domain wall roughening is governed primarily by disorder pinning, even on heating to progressively higher temperatures, followed by a quench. However, the increased energy provided by the thermal cycling does allow accommodation of the artificially straight AFM-written domain walls to the surrounding disorder potential at progressively larger length scales, with the roughness exponent evolution possibly related to a two-to-one dimensional crossover in the behavior of the system. From a comparison of O-poor versus O-rich PZT films, it appears that oxygen vacancies are particularly important for pinning domain walls and allow even relatively small domains to be stabilized at high temperatures, close to T_C. This observation is especially interesting for potential applications, for which, in fact, it may be more useful to have higher oxygen vacancies and, thus, more stable domain structures.

*patrycja.paruch@unige.ch

†Present address: DPA, University of Nebraska-Lincoln, Lincoln, Nebraska 68588, USA.

[1]P. Paruch, T. Giamarchi, and J.-M. Triscone, in *Physics of Ferroelectrics, a Modern Perspective*, edited by K. Rabe, C. H. Ahn, and J.-M. Triscone (Springer, Berlin/Heidelberg, 2007).

[2]E. Agoritsas, V. Lecomte, and T. Giamarchi, Physica B **407**, 1725 (2012).

[3]M. Yamanouchi, D. Chiba, F. Matsukura, T. Dietl, and H. Ohno, Phys. Rev. Lett. **96**, 096601 (2006).

[4]L. Ponson, D. Bonamy, and E. Bouchaud, Phys. Rev. Lett. **96**, 035506 (2006).

[5]S. Lemerle, J. Ferré, C. Chappert, V. Mathet, T. Giamarchi, and P. Le Doussal, Phys. Rev. Lett. **80**, 849 (1998).

[6]G. Blatter, M. V. Feigel'man, V. B. Geshkenbein, A. I. Larkin, and V. M. Vinokur, Rev. Mod. Phys. **66**, 1125 (1994).

[7]T. Giamarchi, in *Quantum Phenomena in Mesoscopic System*, edited by S. I. di Fisica (IOS Press, Amsterdam, 2003).

[8]G. Grüner, Rev. Mod. Phys. **60**, 1129 (1988).

[9]M. Kardar, Physica B **221**, 60 (1996).

[10]J. F. Scott and C. A. P. de Araujo, Science **246**, 1400 (1989).

[11]R. Waser and A. Rüdiger, Nat. Mater. **3**, 81 (2004).

[12]A. K. S. Kumar, P. Paruch, J. M. Triscone, W. Daniau, S. Ballandras, L. Pellegrino, D. Marré, and T. Tybell, Appl. Phys. Lett. **85**, 1757 (2004).

[13]H. Béa and P. Paruch, Nat. Mater. **8**, 168 (2009).

[14]E. K. H. Salje, ChemPhysChem **11**, 940 (2010).

[15]L. F. Cugliandolo, J. Kurchan, J. P. Bouchaud, and M. Mezard, in *Spin Glasses and Random fields*, edited by A. P. Young (World Scientific, Singapore, 1998).

[16]L. F. Cugliandolo, T. Giamarchi, and P. Le Doussal, Phys. Rev. Lett. **96**, 217203 (2006).

[17]G. Schehr and P. L. Doussal, Europhys. Lett. **71**, 290 (2005).

[18]L. F. Cugliandolo, D. R. Grempel, G. Lozano, H. Lozza, and C. A. da Silva Santos, Phys. Rev. B **66**, 014444 (2002).

[19]A. Polkovnikov, K. Sengupta, A. Silva, and M. Vengalattore, Rev. Mod. Phys. **83**, 863 (2011).

[20]A. B. Kolton, A. Rosso, and T. Giamarchi, Phys. Rev. Lett. **95**, 180604 (2005).

[21]S. Bustingorry, L. F. Cugliandolo, and D. Dominguez, Phys. Rev. B **75**, 024506 (2007).

[22]J. L. Iguain, S. Bustingorry, A. B. Kolton, and L. F. Cugliandolo, Phys. Rev. B **80**, 094201 (2009).

[23]A. B. Kolton, A. Rosso, E. V. Albano, and T. Giamarchi, Phys. Rev. B **74**, 140201 (2006).

[24]A. B. Kolton, G. Schehr, and P. Le Doussal, Phys. Rev. Lett. **103**, 160602 (2009).

[25]D. Damjanovic, Phys. Rev. B **55**, R649 (1997).

[26]W. Kleemann, J. Dec, S. Miga, and R. Pankrath, Ferroelectrics **302**, 247 (1998).

[27]T. Tybell, P. Paruch, T. Giamarchi, and J.-M. Triscone, Phys. Rev. Lett. **89**, 097601 (2002).

[28] P. Paruch, T. Giamarchi, and J.-M. Triscone, Phys. Rev. Lett. **94**, 197601 (2005).

[29] P. Paruch, T. Giamarchi, T. Tybell, and J.-M. Triscone, J. Appl. Phys. **100**, 051608 (2006).

[30] B. J. Rodriguez, Y. H. Chu, R. Ramesh, and S. V. Kalinin, Appl. Phys. Lett. **93**, 142901 (2008).

[31] S. Jesse, B. J. Rodriguez, S. Choudhury, A. P. Baddorf, I. Vrejoiu, D. Hesse, M. Alexe, E. A. Eliseev, A. N. Morozovska, J. Zhang, L.-Q. Chen, and S. V. Kalinin, Nat. Mater. **7**, 209 (2008).

[32] V. Likodimos, M. Labardi, and M. Allegrini, Phys. Rev. B **66**, 024104 (2002).

[33] P. Paruch and J.-M. Triscone, Appl. Phys. Lett. **88**, 162907 (2006).

[34] J. Y. Jo, S. M. Yang, T. H. Kim, H. N. Lee, J.-G. Yoon, S. Park, Y. Jo, M. H. Jung, and T. W. Noh, Phys. Rev. Lett. **102**, 045701 (2009).

[35] $Ar:O_2 = 58{:}42$, 180 mTorr and $Ar:O_2 = 80{:}20$, 225 mTorr were used by P.P. and X.H., respectively.

[36] S. V. Kalinin, B. J. Rodriguez, S. Jesse, J. Shin, A. P. Baddorf, P. Gupta, H. Jain, D. B. Williams, and A. Gruverman, Microsc. Microanal. **12**, 206 (2006).

[37] S. Gariglio, N. Stucki, J.-M. Triscone, and G. Triscone, Appl. Phys. Lett. **90**, 202905 (2007).

[38] (A) The 50-nm film was heated for 3-h intervals in 100 °C steps to 485 °C and then in 50 °C steps until domain disappearance at ∼785 °C. The 52- and 91-nm films were heated for 1-h intervals in 100 °C steps to 485 °C and then in 25 °C steps until domain disappearance at ∼625 °C. (B) The 50-nm film was heated for 30-min intervals in 100 °C steps to 300 °C, 50 °C steps to 450 °C, and then 25 °C steps until domain disappearance at ∼525 °C. The 40-nm films were heated for 20-min intervals in 100 °C steps until 400 °C, 50 °C steps until 550 °C, and then 25 °C steps until domain disappearance at ∼625 °C. The 100-nm film was heated for 20-min intervals in 100 °C steps until 200 °C and then 25 °C steps until domain disappearance at ∼325 °C.

[39] T. Nattermann, J. Phys. C **16**, 4125 (1983).

[40] B. Meyer and D. Vanderbilt, Phys. Rev. B **65**, 104111 (2002).

[41] A. I. Larkin, Sov. Phys. JETP **31**, 784 (1970).

[42] P. Zubko, D. J. Jung, and J. F. Scott, J. Appl. Phys. **100**, 114113 (2006).

[43] L. He and D. Vanderbilt, Phys. Rev. B **68**, 134103 (2003).

[44] E. A. Jagla and A. B. Kolton, J. Geophys. Res. **115**, B05312 (2010).

[45] P. Maksymovych, J. Seidel, Y. H. Chu, P. Wu, A. P. Baddorf, L.-Q. Chen, S. V. Kalinin, and R. Ramesh, Nano Lett. **11**, 1906 (2011).

[46] J. Guyonnet, I. Gaponenko, S. Gariglio, and P. Paruch, Adv. Mater. **23**, 5377 (2011).

[47] The significant asymmetry in domain switching and stability as a function of the polarity of the tip bias is a feature already noted in previous studies[46] and can be related to the particular device geometry used. Essentially, the metallic electrodes on either side of the ferroelectric thin films can be considered as two back-to-back Schottky diodes, with the barrier height determined by the work functions of the respective electrode materials.[42,48] In addition, further asymmetry in current-voltage and switching characteristics can result from strain and other boundary-specific conditions and, in thin films, the direction of polarization. Finally, the device architecture itself is strongly asymmetric: One electrode is planar, while the other is the nanoscale AFM tip, with a nominal radius at apex form metal-coated tips given as 25–50 nm. In such devices, the nucleation and growth of domains is, therefore, strongly dependent on the polarity of the voltage applied to the AFM tip.

[48] P. Maksymovych, M. Pan, P. Yu, R. Ramesh, A. P. Baddorf, and S. V. Kalinin, Nanotechnology **22**, 254031 (2011).